Available online at www.sciencedirect.com
ScienceDirect
Journal of Solid State Chemistry 180 (2007) 922–928
JOURNAL OF SOLID STATE CHEMISTRY
www.elsevier.com/locate/jssc

$Li_2Si_3O_7$: Crystal structure and Raman spectroscopy

Hannes Krüger[a,*], Volker Kahlenberg[a], Reinhard Kaindl[b]

[a]*Institute of Mineralogy and Petrography, University of Innsbruck, Innrain 52, 6020 Innsbruck, Austria*
[b]*Christian-Doppler-Laboratory for Advanced Hard Coatings at the Institute of Mineralogy and Petrography, University of Innsbruck, 6020 Innsbruck, Austria*

Received 21 August 2006; received in revised form 19 October 2006; accepted 16 December 2006
Available online 29 December 2006

Abstract

The crystal structure of metastable $Li_2Si_3O_7$ was determined from single crystal X-ray diffraction data. The orthorhombic crystals were found to adopt space group *Pmca* with unit cell parameters of $a = 19.648(3)$ Å, $b = 5.9969(8)$ Å and $c = 4.8691(6)$ Å. The content of the cell is $Z = 4$. The obtained structural model was refined to a *R*-value of 0.035. The structure exhibits silicate sheets, which can be classified as $\{\boldsymbol{uB}, 2, 1^2_\infty\}[Si_6O_{14}]$ using the silicate nomenclature of Liebau. The layers are build up from *zweier* single chains running parallel to *c*. Raman spectra are presented and compared with other silicates. Furthermore, the structure is discussed versus $Na_2Si_3O_7$.

Keywords: Crystal structure; Raman spectroscopy; Lithium trisilicate; X-ray diffraction

1. Introduction

Crystalline lithium silicates are of special importance for certain areas of materials science and solid state chemistry. Recent fields of applications include, for example, glass–ceramics [1], CO_2 absorbing materials [2] and solid electrolytes in lithium batteries [3,4]. With this regard it is interesting to note that the historically first developed glass–ceramic was based on $Li_2Si_2O_5$ [5]. In addition to studies of the crystalline compounds numerous investigations were aimed to elucidate the glass formation and the crystallisation behaviour in the binary glasses of the system Li_2O–SiO_2 [6–8]. Furthermore, the binary glasses have been also used as comparatively simple model systems to understand the internal structure, short range ordering and ion transport mechanisms in amorphous systems [9–12].

According to the phase diagram [13] three thermodynamically stable crystalline phases have to be distinguished: Li_4SiO_4, Li_2SiO_3 and $Li_2Si_2O_5$, respectively. The crystal structures of these compounds are known for a long time. However, there are indications that metastable phases such as $Li_2Si_3O_7$ can be obtained as well. The crystallisation of $Li_2Si_3O_7$ from a stoichiometric glass was firstly reported by Matveev and Velya [14]. A more detailed study was carried out by West and Glasser [15], who gave optical data, IR spectra as well as indexed X-ray powder data along with a suggestion for the space group *Pbcm* or $Pca2_1$ determined from single crystal X-ray photographs. From the geometric similarity between the unit cells of α-$Na_2Si_2O_5$ [16] and $Na_2Si_3O_7$ [17] on the one hand and that between $Li_2Si_2O_5$ [18] and $Li_2Si_3O_7$ on the other hand, they deduced a probable structure for the lithium trisilicate, showing the same type of layers as the sodium trisilicate. Both trisilicates are thermodynamically metastable. Whereas lithium trisilicate is reported to persist indefinitely [15], the sodium compound decomposes within months at ambient conditions [19].

This work reports the crystal structure of $Li_2Si_3O_7$ solved from single crystal X-ray diffraction data, which basically confirms the assumption of West and Glasser [15], although some structural differences will be discussed in detail later. Moreover, the structural investigation is accompanied by a study of the Raman spectra, which includes a discussion of the similarities in the spectra of $Li_2Si_3O_7$ and the mineral orthoenstatite.

*Corresponding author. Fax: +43 512 507 2926.
E-mail address: Hannes.Krueger@uibk.ac.at (H. Krüger).

0022-4596/$ - see front matter © 2007 Elsevier Inc. All rights reserved.
doi:10.1016/j.jssc.2006.12.015

2. Experimental details

2.1. Synthesis

The synthesis of lithium trisilicate was carried out following the procedure given in [15]. Fine grained Li_2CO_3 (Merck, p.a.) and SiO_2 (Alfa Johnson Matthey, 99.995%) were mixed according to the stoichiometric ratio of lithium trisilicate and filled in a platinum crucible. The sample was inserted in a resistance heated chamber furnace at 673 K. The furnace was then heated up to 1673 K using a rate of 5 K/min and held at this temperature for about 30 min. Subsequently, the sample was quickly transferred to another chamber furnace, pre-heated at 1163 K. While inserting the sample, the temperature of the second furnace dropped temporarily down to approximately 1020 K, but stabilised after 1 min at 1163 K. Because of the thermal inertia of the crucible/sample, the sample temperature probably has not dropped that low. The sample was kept for 6 min at 1163 K, before it was finally removed from the furnace and cooled to ambient conditions. After coarsely crushing the sample, transparent crystals, exhibiting shapes of very thin platelets, could be isolated from the bulk material for further single crystal investigations. A part of the bulk material was powderised and scrutinised by means of X-ray powder diffraction, which revealed $Li_2Si_3O_7$, as well as the stable form of $Li_2Si_2O_5$ [20] and minor amounts of quartz as by-products. The phase amounts (wt%) as roughly determined by Rietveld analysis were 56, 42 and 2, respectively. West and Glasser [15] reported, that the trisilicate crystallises in a temperature range of 1123–1193 K. Samples cooled below 1123 K were reported to show greatly reduced yields of $Li_2Si_3O_7$. Higher amounts of the trisilicate may be obtained by optimising the thermal treatment.

2.2. Single crystal X-ray diffraction

One of the selected crystals was mounted at the top of a glass fibre for single crystal X-ray diffraction experiments on a STOE IPDS II diffractometer. Table 1 presents further experimental details. The diffraction pattern could be indexed with an orthorhombic lattice. The data reduction process included corrections for Lorentz, polarisation and air absorption effects [21]. Due to the pronounced anisotropic shape of the thin crystal a correction for absorption was performed by the integration method using eight indexed crystal faces [22]. An internal R value of 0.049 for the Laue group *mmm* confirmed the orthorhombic symmetry. From the analysis of systematically absent reflections the extinction symbol *P-ca* could be derived. Possible space groups are $P2_1ca$ (No. 29) or centrosymmetric *Pmca* (No. 57). The structure was solved in *Pmca* using direct methods [23] and refined using the software *Jana2000* [24]. The non-standard setting of the cell was chosen to stay conform to earlier structural investigations on trisilicates [17,19]. The refinement of atomic coordinates (Table 2) as well as anisotropic displacement parameters[1] of all atoms results in the final structural model.

Table 1
Experimental details

Crystal data	
Chemical formula	$Li_2Si_3O_7$
M_r	210.13
Cell setting, space group	Orthorhombic, *Pmca*
Temperature (K)	298
a, b, c (Å)	19.648(3), 5.9969(8), 4.8691(6)
V (Å^3)	573.70 (14)
Z	4
D_x (Mg m^{-3})	2.435
Radiation type	Mo K_α
No. of reflections for cell parameters	3544
θ range (°)	2.1–29.5
μ (mm^{-1})	0.81
Crystal form, colour	Plate, colourless
Crystal size (mm)	0.26 × 0.09 × 0.02
Data collection	
Diffractometer	STOE IPDS 2
Data collection method	Rotation method
Absorption correction	Integration
T_{min}	0.875
T_{max}	0.983
No. of measured, independent and observed reflections	4610, 803, 649
Criterion for observed reflections	$I > 3\sigma(I)$
R_{int} (mmm)	0.049
θ_{max} (°)	29.2
Range of h, k, l	$-26 \leqslant h \leqslant 26$ $-8 \leqslant k \leqslant 8$ $-6 \leqslant l \leqslant 6$
Refinement	
Refinement on	F
$R[F^2 > 2\sigma(F^2)], wR(F^2), S$	0.035, 0.040, 2.34
No. of reflections	803 reflections
No. of parameters	59
Weighting scheme	Based on measured s.u.'s $w = 1/(\sigma^2(F) + 0.0001F^2)$
$(\Delta/s)_{max}$	<0.0001
$\Delta\rho_{max}, \Delta\rho_{min}$ (e Å^3)	0.53, −0.50
Extinction method	B-C type 1 Gaussian isotropic [49]
Extinction coefficient ($\times 10^{-2}$)	4(2)

Software used: STOE *X-Area*, *X-Red* [21,22]; *Sir97* [23]; *Jana2000* [24]; *DRAWxtl* [50].

Table 2
Positional parameters

Atom	x	y	z	U_{iso}
Si1	0.25	0.34929(15)	0.57981(18)	0.0123(2)
Si2	0.10440(3)	0.14615(10)	0.55364(12)	0.01098(16)
O1	0.05547(8)	0.3389(3)	0.4566(3)	0.0156(4)
O2	0.18419(9)	0.2016(3)	0.5144(4)	0.0194(5)
O3	0.25	0.4260(4)	0.8970(5)	0.0206(7)
O4	0.09068(8)	0.0865(3)	0.8801(3)	0.0141(4)
Li1	0.0440(2)	0.3535(7)	0.0567(9)	0.0190(11)

[1] A table of anisotropic displacement parameters has been deposited and can be accessed from the online version of this article.

2.3. Raman spectroscopy

Confocal Raman spectra were obtained with a HORIBA JOBIN YVON LabRam-HR 800 Raman micro-spectrometer. Samples were excited by the 487.9 nm emission line of a 30 mW Ar^+-laser and an OLYMPUS 100× objective (N.A. = 0.9). The spectra were recorded without polarisation filter for the incident laser and the scattered Raman light. Size and power of the laser spot on the surface was approximately 1 μm and 5 mW. The spectral resolution, determined by measuring the Rayleigh line, was about 1.8 cm^{-1}. The dispersed light was collected by a 1024 × 256 open electrode CCD detector. Confocal pinhole was set to 1000 μm. Spectra were recorded unpolarised in scanning-mode [25,26]. All spectra were background corrected by subtraction of line segments and fitted to Gauss–Lorentz functions. Accuracy of Raman line shifts, calibrated by regular measuring the Rayleigh line, was in the order of 0.5 cm^{-1}. Simple symmetry analysis was done by the aim of the web-based program package *SAM* [27].

3. Description of the structure

The structure contains two symmetrically independent silicon atoms, which are each four-coordinated by oxygen atoms. The coordination tetrahedra of the two silicon atoms form a *zweier* single chain [28] each. The smallest identity period of the structure along [0 0 1] represents the direction of the chains (Fig. 1). In Fig. 2a it is shown how these chains are connected to build $[Si_3O_7]^{2-}$-layers. The darker chain is formed by Si1 and as the 'central' chain in the layer the connectivity of its tetrahedra is Q^4. The oxygen O2 is shared by the different chains. Tetrahedra belonging to the 'outer' chain (formed by Si2, light grey in the figures) are Q^3-connected and their O1 is not shared between silicon tetrahedra. Therefore, the bonding distance Si2–O1 is significantly shorter (see Table 3) compared to an average Si–O bonding distance [28]. This shorter bond to the terminal oxygen O1 induces a higher distortion of the Q^3- compared to the Q^4-tetrahedra. A quantitative measure of the distortion is proposed by a work of Robinson et al. [29]. The mean tetrahedral quadratic elongation $\langle\lambda_{tet}\rangle$ is 1.001(1) and 1.002(1), the tetrahedral angle variance $\sigma^2_{\theta(tet)}$ is 2.8(1) and 9.8(2) for the Q^4- and Q^3-tetrahedra, respectively. A difference in the distortion parameters of Q^3- and Q^4-species in a layered silicate structure was also observed in $Na_6Si_8O_{19}$ [30]. However, the observed distortion parameters are in good agreement with the linear correlation between $\sigma^2_{\theta(tet)}$ and $\langle\lambda_{tet}\rangle$ observed by Robinson et al. for a variety of silicates and aluminosilicates [29]. Distances, angles and bond valence sums [31] are given in Table 3.

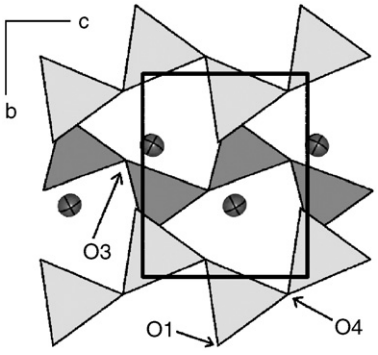

Fig. 1. Silicate *zweier* single chains of a single $[Si_6O_{14}]$ layer. Dark tetrahedra represent Si1, the brighter tetrahedra represent Si2 coordination polyhedra. The displayed region extends from $x = 0$ to 0.5. Li displacement ellipsoids are drawn at 95% probability.

Table 3
Distances and angles

Atoms	Distance (Å)	Angle (°)	BVS
Si1–O2	1.5993(19)		
Si1–O2^{i}	1.5993(19)		
Si1–O3	1.612(3)		
Si1–O3^{ii}	1.615(3)		
O2–Si1–O2^{i}		107.88(10)	
O2–Si1–O3		110.43(9)	
O2–Si1–O3^{ii}		110.63(9)	
O2^{i}–Si1–O3		110.43(9)	
O2^{i}–Si1–O3^{ii}		110.63(9)	
O3–Si1–O3^{ii}		106.86(14)	
Si1			4.20(1)
Si2–O1	1.5759(18)		
Si2–O2	1.6139(19)		
Si2–O4	1.6515(17)		
Si2–O4^{iii}	1.6531(18)		
O1–Si2–O2		113.96(10)	
O1–Si2–O4		110.36(9)	
O1–Si2–O4^{iii}		111.47(9)	
O2–Si2–O4		108.50(9)	
O2–Si2–O4^{iii}		105.77(9)	
O4–Si2–O4^{iii}		106.41(9)	
Si2			4.02(1)
Li1–O1	1.962(5)		
Li1–O1^{ii}	1.921(5)		
Li1–O1^{iv}	1.957(4)		
Li1-O4^{v}	2.036(5)		
O1–Li1–O1^{ii}		106.3(2)	
O1–Li1–O1^{iv}		98.4(2)	
O1–Li1–O4^{v}		109.4(2)	
O1^{ii}–Li1–O1^{iv}		98.7(2)	
O1^{ii}–Li1–O4^{v}		126.5(2)	
O1^{iv}–Li1–O4^{v}		113.6(2)	
Li1			1.033(7)

Symmetry codes: (i) $\frac{1}{2}-x, y, z$; (ii) $x, 1-y, -\frac{1}{2}+z$; (iii) $x, -y, -\frac{1}{2}+z$; (iv) $x, y, -1+z$; (v) $-x, y, \frac{1}{2}-z$.

The lithium atoms are located between the silicate layers and are also four-coordinated by oxygens. The coordination tetrahedra involve three oxygen atoms belonging to the closest silicate layer, the fourth one is attributed to the other neighbouring layer. Compared to the silicate tetrahedra, they are highly distorted [$\sigma^2_{\theta(tet)} = 111(1)$]. The $[LiO_4]$-tetrahedron also forms chains (see Fig. 3), but the

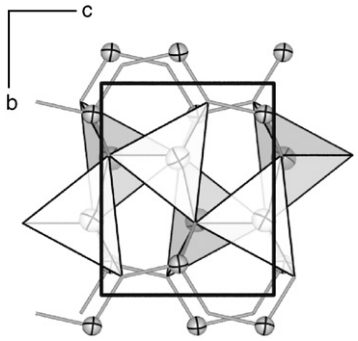

Fig. 3. Chain of [LiO_4] coordination tetrahedra including their bonds to silicon atoms. The displayed region extends from $x = 0.3$ to 0.8. Coordination tetrahedra are displayed transparent. Displacement ellipsoids are shown at 95% probability.

[LiO_4] tetrahedra of adjacent chains share edges, so that their linkedness is two. Since each tetrahedron shares two corners and two edges with neighbouring ones, its connectedness is four with regard to [LiO_4] tetrahedra. The one unshared oxygen exhibits the longest Li–O distance (see Table 3).

4. Results of the Raman spectroscopy

The Raman spectrum of a thin, sheet-like $Li_2Si_3O_7$ crystal is given in Fig. 4. Raman shifts and relative intensities in percent, related to the amplitude of the most intense Raman band at 387 cm^{-1}, are listed in Table 4. Thirty Raman bands with relative intensities $\geqslant 1$ could be detected. The high-wavenumber region of the spectrum from 800 to 1300 cm^{-1} contains two intense bands at 928 and 1097 cm^{-1} and five bands of lower intensity. The mid- and low-wavenumber regions below 800 cm^{-1} show two bands of almost 100% relative intensity at 387 and 516 cm^{-1} and several other bands (139, 150, 307, 359 cm^{-1}) with intensities around 20%. A large number of low-intensities bands occur below 300 cm^{-1}, some also at higher wavenumbers. The theoretical number of possible vibrational modes of $Li_2Si_3O_7$, which crystallises in the space group *Pmca* (point group *mmm* or D_{2h}) can be deduced by symmetry analysis using the web-based program package *SAM* [27]. One hundred and twenty-seven vibrational modes are possible according to the following irreducible representations:

$$\Gamma_{Vib} = 19A_g + 19B_{1g} + 17B_{2g} + 17B_{3g} + 17B_{1u} + 19B_{2u} + 19B_{3u}.$$

Seventy-two of them (all *g*-modes) are Raman and the rest are IR-active. Band assignment to vibrational modes can be done by analogy by comparing $Li_2Si_3O_7$ with the spectra of known related structures. Bands of alkali and alkaline earth metal silicates in the high-wavenumber range 800–1300 cm^{-1} are generally caused by symmetric stretching vibrations of the SiO_4 groups (ν_{Si-O}) [32,33]. The vibrational wavenumber of these modes is approximately

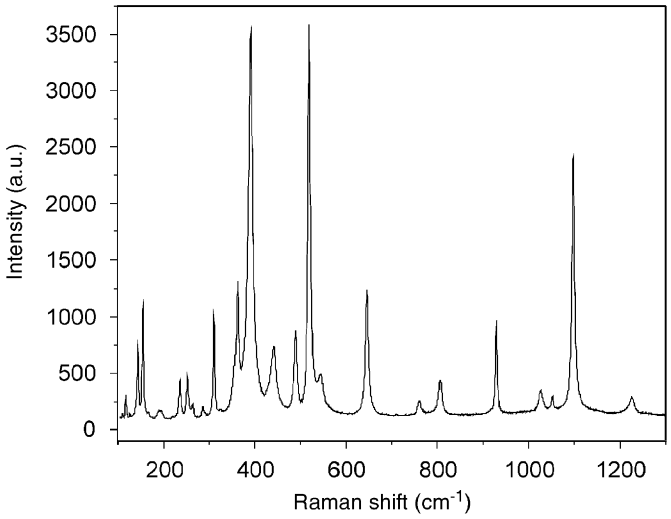

Fig. 4. Raman spectrum of a thin plate-like crystal of $Li_2Si_3O_7$.

related to the type of the silicon–oxygen tetrahedron and to the different structural building units [32–35].

Experimental and theoretical studies of binary sodium silicates suggest that the intense band at 1097 cm^{-1} results from ν_{Si-O} of tetrahedra with three bridging oxygens (Q^3) [33]. In pyroxenes and $NaYSi_2O_6$, which are based on *zweier* and *vierer* single chains, modes between 1000 and 1050 cm^{-1} were observed and assigned to symmetric and asymmetric Si–O stretching vibrations of tetrahedra with non-bridging oxygens in the chains [36–38]. The mode frequencies of ν_{Si-O} of $Li_2Si_3O_7$ are slightly higher compared to the chain silicate orthoenstatite (Table 4), consistent with slightly lower Si–O bond lengths between 1.58 and 1.65 Å. $Na_6Si_8O_{19}$, which consists of four different *zweier* single chains forming a sequence of tetrahedral layers, shows a ν_{Si-O} mode with extremely high intensity at 1060 cm^{-1} [30]. Q^4-species are Raman inactive in the high wavenumber range, but the high intensity of the ν_{Si-O} mode at 1097 cm^{-1} may be attributed to increased intensities of Q^3-species with adjacent Q^4-species [33].

In the intermediate wavenumber range 400–900 cm^{-1}, high-intensity Raman bands emerge by the symmetric bending and rocking vibrations of the Si–O–Si ($\delta_{Si-O-Si}$) and ν_{Si-O} of the Si–O bridging oxygen of adjacent SiO_4 tetrahedra [33,36,37,39,40]. Also bending modes of the non-bridging oxygens (δ_{Onb}) contribute to bands in this spectral region [39,41]. For binary sodium silicates, a relation between the $\delta_{Si-O-Si}$ vibrational wavenumber and the Si–O–Si angle was established [33]. According to them, $\delta_{Si-O-Si}$ are expected around 600–700 cm^{-1}, corresponding to the angle variation in the two Q^3- and Q^4-connected chains of $Li_2Si_3O_7$ of 130–140°. In $Li_2Si_3O_7$ several bands from 438 to 643 cm^{-1} with relative intensities between 10 and 97 were observed. In orthoenstatite, two strong modes at 663 and 687 cm^{-1} correspond to two kinds of tetrahedral chains with 19° kinking angles apart (Table 4) [36]. Several intense bands between 480 and 540 cm^{-1} were described in the spectrum of $Na_6Si_8O_{19}$, which consists of a sequence of

Table 4
Raman shifts (cm^{-1}) and intensities (amplitude) of bands in the spectrum of $Li_2Si_3O_7$ (Lith.) in percent relative to the highest intensity band at 387 cm^{-1}, compared with experimental data of orthoentstatite (En.) [36] and $Na_6Si_8O_{19}$ (Sod.) [30]

Lith.	Int.	En.	Sod.	Int.	Lith.	Int.	En.	Sod.	Int.
106	1	–	107	7	–	–	–	481	59
113	6	113(w)	–	–	486	21	475(w)	486	10
123	1	–	123	6	–	–	–	494	92
139	19	132(m)	–	–	516	97	516(w)	511	45
150	27	–	149	4	–	–	519(m)	–	–
153	2	154(w)	–	–	521	8	525(w)	–	–
–	–	160(w)	–	–	–	–	527(w)	–	–
163	1	165(w)	167	18	541	10	545(w)	540	54
189	2	193(w)	178	3	–	–	538(w)	–	–
–	–	196(m)	196	4	–	–	552(w)	569	8
–	–	–	204	6	–	–	581(m)	–	–
–	–	–	226	12	–	–	595(sh)	–	–
232	10	234(m)	232	5	643	33	–	–	–
–	–	237(w)	–	–	–	–	663(s)	706	3
–	–	242(w)	–	–	–	–	687(s)	–	–
248	10	243(m)	248	3	759	4	750(w)	766	14
259	3	–	–	–	804	9	–	–	–
283	2	–	288	2	–	–	846(w)	–	–
–	–	301(w)	–	–	–	–	891(w)	–	–
307	27	306(w)	–	–	928	25	927(m)	927	<1
–	–	322(w)	324	5	–	–	960(m)	964	5
–	–	339(w)	–	–	–	–	–	975	3
352	7	343(s)	–	–	–	–	–	995	12
359	29	358(w)	356	86	–	–	1014(sh)	–	–
–	–	379(w)	361	22	1026	5	1033(s)	1027	7
387	100	403(s)	381	3	–	–	1043(m)	1049	24
–	–	409(w)	412	4	1051	4	1062(w)	1060	100
–	–	419(w)	–	–	1097	67	–	1095	11
–	–	422(s)	–	–	1106	2	–	1109	12
438	17	442(w)	–	–	–	–	–	1130	10
–	–	448(m)	453	4	–	–	–	1177	7
–	–	460(w)	–	–	1226	4	–	–	–

Abbreviations: weak (w), medium (m), strong (s), shoulder (sh).

tetrahedral layers built up by *zweier* single chains and shows a considerable scatter in Si–O–Si angles from 136° to 161° [30]. We therefore suggest the band at 643 cm^{-1} to be related to ν_{Si-O} of both chains, which does not split due to the low angle variations. The other bands in this wavenumber region correspond probably to $\delta_{Si-O-Si}$ or to δ_{Onb} vibrations of the Si–O layers.

In the low wavenumber range below 400 cm^{-1}, Raman active vibrations are caused by lattice vibrations of the framework and by the bonding of cation and oxygen (Li–O) [33]. Raman shifts and intensities of bands in that range are similar to orthoenstatite and $Na_6Si_8O_{19}$ (Table 4) [36], supporting that lattice vibrations of both the layers and the *zweier* single chains they are composed of contribute to the spectrum in that range.

The most frequent full width at half maximum of virtually all Raman bands around 10 cm^{-1} and a maximum $<20\ cm^{-1}$ and the presence of bands $<400\ cm^{-1}$ indicate a well ordered structure, long-distance ordering and the absence of structural disorder like short-range Si–O–Si bridging angle disorder in sodium silicate glasses [33,42].

5. Related structures and discussion

The type of $[Si_6O_{14}]$-layers found in $Li_2Si_3O_7$ is topologically equivalent to the silicate sheets found in $Na_2Si_3O_7$ [17]. A more recent study [19] showed that the sodium trisilicate structure is more complex involving aperiodic changes in the orientation of the 'central' chain. However, the classification of the silicate layer after Liebau's nomenclature [28,43] should be the same for both structures. A classification of the $Li_2Si_3O_7$ structure utilising the software CRYSTANA [44,45] ranks the chains in $Li_2Si_3O_7$ as unbranched, thus leading to $Li_4\{\boldsymbol{uB}, 2, 1^2_\infty\}[Si_6O_{14}]$ as the structural formula after Liebau.

As already mentioned, the compound $Na_2Si_3O_7$ exhibits very similar layers. As can be seen in Fig. 2a, the chains of one layer in $Li_2Si_3O_7$ are all of the same type, e.g. their vertices connecting along the chain direction point in the same direction for one layer. The neighbouring layer is equivalent by a centre of symmetry. Therefore, the connecting vertices point to the opposite direction. In the sodium compound (see Fig. 2b) the centre of symmetry is

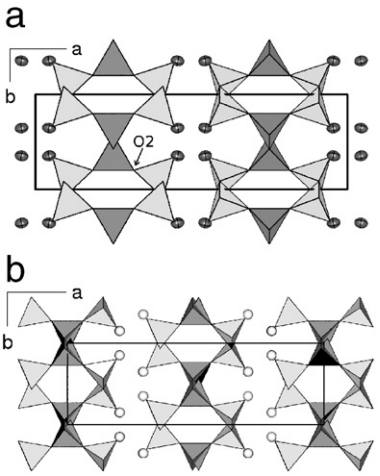

Fig. 2. $[Si_6O_{14}]$ layers formed by two independent *zweier* single chains. (a) In $Li_2Si_3O_7$, lithium atoms represented by 95% probability displacement ellipsoids. Dark and bright tetrahedra represent Si1 and Si2 coordination polyhedra, respectively. (b) Different arrangement of the layers and two distinct orientations of the central chain in the averaged structure of modulated $Na_2Si_3O_7$ [19]. Sodium atoms depicted by spheres.

located within the 'central' chain. Consequently the connecting vertices of the 'outer' chains of one layer point in opposite directions. The 'central' chain can adopt two equivalent orientations. The sequence of these orientations within one layer shows aperiodic order and breaks the lattice periodicity along the *b* direction. A detailed description of the incommensurate structure of the metastable sodium trisilicate can be found in [19]. The larger sodium atoms between the layers are coordinated by five oxygens causing a different configuration of the $[Si_6O_{14}]$ sheets in the sodium compound. An interesting subject for further investigations is a possible solid solution series between the sodium and the lithium compound as found in the metasilicates (although very limited) [46].

Two more compounds are known, which may adopt similar $[Si_6O_{14}]$ silicate sheets. $Na_2Cu(Si_3O_7)_2 \cdot 5H_2O$ [47], which shows a doubled *b* and *c* lattice parameter (compared to $Li_2Si_3O_7$). This could be caused by the presence of *vierer* chains in the more complex layer. The incorporation of water molecules and copper atoms between the silicate anions may be expressed by the increased lattice parameter *a*. The second compound was described by Guth et al. [48]: a hydrated compound ($H_2Si_3O_7$), which is reported to show two different modifications. Although there are good indications, that these compounds adopt similar silicate layers, the final evidence of structural investigations is still outstanding.

Acknowledgments

The authors are grateful to Friedrich Liebau for very helpful discussion regarding the classification of the silicate layer. Furthermore, the authors would like to thank three anonymous referees, whose valuable comments improved the paper.

Appendix A. Supplementary data

Supplementary data associated with this article can be found in the online vesion at 10.1016/j.jssc.2006.12.015.

References

[1] W. Höland, G. Beall, Glass Ceramic Technology, The American Ceramic Society, 2002.
[2] K. Essaki, N. Nakagawa, K. Kato, H. Uemoto, CO_2 absorption by lithium silicate at room temperature, J. Chem. Eng. Jpn. 37 (2004) 772–777.
[3] K. Jackowska, A.R. West, Ionic conductivity of Li_4SiO_4 solid solutions in the system Li_2O–Al_2O_3–SiO_2, J. Mater. Sci. 18 (8) (1983) 2380–2384.
[4] A. Khorassani, A.R. West, Lithium (1^+) ion conductivity in the lithium silicate–lithium vanadate(V) system, J. Solid State Chem. 53 (3) (1984) 369–375.
[5] S.D. Stookey, Chemical machining of photosensitive glass, Ind. Eng. Chem. 45 (1953) 115–118.
[6] W. Vogel, Struktur und Kristallisation der Gläser, Verlag für Grundstoffindustrie, Leipzig, Germany, 1963.
[7] P.W. McMillan, Glass-Ceramics, second ed., Academic Press, New York, 1979.
[8] P.F. James, Kinetics of crystal nucleation in silicate glasses, J. Non-Cryst. Solids 73 (1985) 517–540.
[9] W. Beier, G.H. Frischat, Lithium self-diffusion in lithium silicate glasses, Glastech. Ber. 57 (1984) 71–80.
[10] J. Habasaki, Y. Hiwatari, Molecular dynamics study of the mechanism of ion transport in lithium silicate glasses: characteristics of the potential energy surface and structures, Phys. Rev. B 69 (2004) 144207/1–8.
[11] H. Lammert, M. Kunow, A. Heuer, Complete identification of alkali sites in ion conducting lithium silicate glasses: a computer study of ion dynamics, Phys. Rev. Lett. 90 (2003) 215901/1–4.
[12] L.G. Soltay, G.S. Henderson, Structural differences between lithium silicate and lithium germanate glasses by Raman spectroscopy, Phys. Chem. Glasses 46 (2005) 381–384.
[13] E.M. Levin, C.R. Robbins, H.F. McMurdie, Phase Diagrams for Ceramists, The American Ceramic Society, 1969.
[14] M.A. Matveev, V.V. Velya, The crystallization of lithium glasses of the system Li_2O–SiO_2, Steklo Keram. 16 (10) (1959) 14–20.
[15] A.R. West, F.P. Glasser, Crystallization of lithium trisilicate, $Li_2Si_3O_7$, from lithium oxide–silicon dioxide melts, Mater. Res. Bull. 5 (9) (1970) 837–842.
[16] F. Liebau, Untersuchungen an Schichtsilikaten des Formeltyps $A_m(Si_2O_5)_n$. II. Über die Kristallstruktur des α-$Na_2Si_2O_5$, Acta Crystallogr. 14 (1961) 395–398.
[17] P.B. Jamieson, Crystal structure of $Na_2Si_3O_7$: a new type of silicate sheet, Nature 214 (1967) 794–796.
[18] F. Liebau, Untersuchungen an Schichtsilikaten des Formeltyps $A_m(Si_2O_5)_n$. I. Die Kristallstruktur der Zimmertemperaturform des $Li_2Si_2O_5$, Acta Crystallogr. 14 (1961) 389–395.
[19] H. Krüger, V. Kahlenberg, K. Friese, $Na_2Si_3O_7$: an incommensurate structure with crenel-type modulation functions, refined from a twinned crystal, Acta Crystallogr. B 62 (3) (2006) 440–446.
[20] B.H.W.S de Jong, H.T.J. Supèr, A.L. Spek, N. Veldman, G. Nachtegaal, J.C. Fischer, Mixed alkali systems: structure and ^{29}Si MASNMR of $Li_2Si_2O_5$ and $K_2Si_2O_5$, Acta Crystallogr. B 54 (1998) 568–577.
[21] STOE & Cie GmbH, X-Area, Darmstadt, 2005.
[22] STOE & Cie GmbH, X-Red, Darmstadt, 2005.
[23] A. Altomare, M.C. Burla, M. Camalli, G. Cascarano, C. Giacovazzo, A. Guagliardi, A.G.G. Moliterni, G. Polidori, R. Spagna, SIR97: a new program for solving and refining crystal structures, Bari, Italy, 1997.

[24] V. Petříček, M. Dušek, L. Palatinus, Jana2000, The crystallographic computing system, Institute of Physics, Prague, Czech Republic, 2000.
[25] P. Knoll, R. Singer, W. Kiefer, Improving spectroscopic techniques by a scanning multichannel method, Appl. Spectrosc. 44 (5) (1990) 776–782.
[26] L. Nasdala, H.-J. Massonne, Microdiamonds from the Saxonian Erzgebirge, Germany: in situ micro-Raman characterisation, Eur. J. Mineral. 12 (2) (2000) 495–498.
[27] M.I. Aroyo, J.M. Perez-Mato, C. Capillas, E. Kroumova, S. Ivantchev, G. Madariaga, A. Kirov, H. Wondratschek, Bilbao crystallographic server: I. Databases and crystallographic computing programs, Z. Kristallogr. 221 (1) (2006) 15–27.
[28] F. Liebau, Structural Chemistry of Silicates—Structure, Bonding, and Classification, Springer, Berlin, 1985.
[29] K. Robinson, G.V. Gibbs, P.H. Ribbe, Quadratic elongation: a quantitative measure of distortion in coordination polyhedra, Science 172 (1971) 567–570.
[30] H. Krüger, V. Kahlenberg, R. Kaindl, Structural studies on $Na_6Si_8O_{19}$—a monophyllosilicate with a new type of layered silicate anion, Solid State Sci. 7 (11) (2005) 1390–1396.
[31] I.D. Brown, D. Altermatt, Bond-valence parameters obtained from a systematic analysis of the inorganic crystal structure database, Acta Crystallogr. B 41 (1985) 244–247.
[32] M. Akaogi, N.L. Ross, P. McMillan, A. Navrotsky, The Mg_2SiO_4 polymorphs (olivine, modified spinel and spinel)-thermodynamic properties from oxide melt solution calorimetry, phase relations, and models of lattice vibrations, Am. Mineral. 69 (1984) 499–512.
[33] J.-L. You, G.-C. Jiang, H.-Y. Hou, H. Chen, Y.-Q. Wu, K.-D. Xu, Quantum chemistry study on superstructure and Raman spectra of binary sodium silicates, J. Raman Spectrosc. 36 (3) (2005) 237–249.
[34] S.K. Sharma, D. Virgo, B. Mysen, Structure of glasses and melts of $Na_2O \cdot xSiO_2$ ($x = 1, 2, 3$) composition from Raman spectroscopy, Year Book 77, Carnegie Institution of Washington 1978, pp. 649–652.
[35] Y. Iguchi, S. Kashio, T. Goto, Y. Nishina, T. Fuwa, Raman spectroscopic study on the structure of silicate slags, Can. Metall. Q. 20 (1) (1981) 51–56.
[36] N. Choudhury, S. Ghose, C.P. Chowdhury, C.K. Loong, S.L. Chaplot, Lattice dynamics, Raman spectroscopy, and inelastic neutron scattering of orthoenstatite $Mg_2Si_2O_6$, Phys. Rev. B 58 (2) (1998) 756–765.
[37] H. Yang, L.W. Finger, P.G. Conrad, C.T. Prewitt, R.M. Hazen, A new pyroxene structure at high pressure: single-crystal X-ray and Raman study of the *Pbcn*–$P2_1cn$ phase transition in protopyroxene, Am. Mineral. 84 (1999) 245–256.
[38] D.M. Többens, V. Kahlenberg, R. Kaindl, Characterization and ab initio XRPD structure determination of a novel silicate with vierer single chains: the crystal structure of $NaYSi_2O_6$, Inorg. Chem. 44 (25) (2005) 9554–9560.
[39] C. Karlsson, E. Zanghellini, J. Swenson, B. Roling, D.T. Bowron, L. Börjesson, Structure of mixed alkali/alkaline-earth silicate glasses from neutron diffraction and vibrational spectroscopy, Phys. Rev. B 72 (2005) 064206/1–12.
[40] R.J. Kirkpatrick, J.L. Yarger, P.F. McMillan, P. Yu, X. Cong, Raman spectroscopy of C-S-H, tobermorite, and jennite, Adv. Cem. Based Mater. 5 (3–4) (1997) 93–99.
[41] R.J. Bell, P. Dean, D.C. Hibbins-Butler, Normal mode assignments in vitreous silica, germania and beryllium fluoride, J. Phys. C Solid State 4 (10) (1971) 1214–1220.
[42] N. Zotov, M. Marinov, L. Konstantinov, Degree of structural disorder in sodium metasilicate glass: model for Raman spectra, J. Non-Cryst. Solids 197 (1996) 179–191.
[43] J. Lima-de-Faria, E. Hellner, F. Liebau, E. Makovicky, E. Parthé, Nomenclature of inorganic structure types. Report of the International Union of Crystallography commission on crystallographic nomenclature subcommittee on the nomenclature of inorganic structure types, Acta Crystallogr. A 46 (1) (1990) 1–11.
[44] H.-J. Klein, CRYSTANA: Liebau classification and ring statistics, ⟨http://www.is.informatik.uni-kiel.de:8081⟩, 2001.
[45] K. Goetzke, H.-J. Klein, P. Kandzia, Automatic crystal chemical classification of silicates using direction-labeled graphs, in: Proceedings of the WG 87 Workshop on Graph-theoretic Concepts in Computer Science, Lecture Notes in Computer Science, vol. 314, Springer, Berlin, 1988, pp. 242–254.
[46] A.R. West, Phase equilibria in the system Na_2SiO_3–Li_2SiO_3, J. Am. Ceram. Soc. 59 (3–4) (1976) 118–121.
[47] Y. Hubert, D. Jordan, J.-L. Guth, A. Kalt, Crystallographic characteristics of two new synthetic copper sodium silicates, C. R. Seances Acad. Sci., Ser. D Sci. Nat. 284 (5) (1977) 329–332.
[48] J.-L. Guth, Y. Hubert, D. Jordan, A. Kalt, B. Perati, R. Wey, A new type of crystalline hydrated silica, of formula $H_2Si_3O_7$, C. R. Seances Acad. Sci., Ser. D Sci. Nat. 285 (16) (1977) 1367–1370.
[49] P.J. Becker, P. Coppens, Extinction within the limit of validity of the Darwin transfer equations. I. General formalism for primary and secondary extinction and their applications to spherical crystals, Acta Crystallogr. A 30 (1974) 129–147.
[50] L.W. Finger, M. Kroeker, B. Toby, DRAWxtl V5.1, ⟨http://www.lwfinger.net/drawxtl⟩, 2005.